Spark plasma sintering of nanostructured ZnS ceramics: Grain growth control and improved hardness

Damien Bregiroux, Julie Cedelle

Version of Record: https://www.sciencedirect.com/science/article/pii/S0921509321013289
Manuscript_8ca75d0bd4b01a1a678f423589348c98

Spark plasma sintering of nanostructured ZnS ceramics: grain growth control and improved hardness

Damien Bregiroux[1,*], Julie Cedelle[2]

[1] Sorbonne Université, CNRS, Chimie de la Matière Condensée de Paris, LCMCP, F-75005 Paris, France

[2] Laboratoire LEME, UPL, Univ Paris Nanterre, 50 rue de Sèvres, 92410 Ville d'Avray, France

* Corresponding author. Tel.: + 331 442 75679

E-mail address: damien.bregiroux@sorbonne-universite.fr (D. Bregiroux)

Abstract

The densification and grain growth behavior of a ZnS nanopowder during spark plasma sintering (SPS) were investigated under the pressure of 125 MPa and constant heating rate of 25 °C min^{-1}. At a sintering temperature of 550 °C, almost fully dense ZnS ceramics (98.2%) could be obtained with grain size as low as 75 nm. At higher temperature, ZnS is subject of a very important grain growth that is detrimental to the mechanical properties. A maximum Vickers microhardness of 4.2 GPa was measured, which is 70 % higher than the current state of the art. Retaining the grain size below 100 nm appears to be the key to developing competitive ZnS functional ceramics.

Keywords

Spark plasma sintering, nanocrystalline microstructure, grain growth, mechanical properties, zinc sulfide

Based on cheap and abundant elements, zinc sulfide ZnS is a very attractive material. Zinc sulfide exists in two main crystalline forms: a cubic one, named blende or sphalerite, and a hexagonal one, known as wurtzite [1]. In both structures, Zn^{2+} and S^{2-} ions are in tetrahedral environment. The cubic to hexagonal transformation occurs around 1020°C [2,3]. ZnS is a wide bandgap (3.6–3.9 eV) II–VI semiconductor compound with versatile properties in the fields of optics, photocatalysis, electronics, chemical sensors, biosensors and nanogenerators [4,5]. ZnS is used in the bulk ceramic form in the field of optical material for IR windows or as laser gain media operating over the mid-infrared (2–5 μm) spectral region [6-8]. For such applications, materials are subject to significant mechanical stresses, as impact or erosion, and temperature gradients [9-11]. Thus, mechanical properties of the ceramics are of prime importance. These properties are known to be strongly dependent on the microstructure, and therefore the manufacturing process, mainly the nature of the starting powder, the shaping and the sintering steps [12,13]. ZnS ceramics suffer from poor mechanical properties compared to other IR ceramics (*e.g.* $MgAl_2O_4$, Y_2O_3). According to the existing literature, Vickers hardness and fracture toughness are in the range of 1.5 to 2.5 GPa and 0.8 to 1.4 $MPa.m^{-1/2}$, respectively, depending on the mean grain size (2.5 to 20 μm for CVD ZnS ceramics) [10,14]. Improving these properties is thus strategic and could be performed by a better control of the nanostructural nature of the microstructure. Without additive or external pressure, ZnS powder is very difficult to sinter, probably because the non-densifying vapor diffusion mechanism is predominant at high temperature. To our knowledge, only one paper reports that dense ZnS ceramics (*i.e.* > 98 % of the theoretical density) can be obtained by

conventional sintering under N_2 without additive [15]. Surprisingly, no other work has since been published based on this article. Our own attempts to reproduce these experiments were also failed. Recently, Yin *et al.* obtained 90 % dense ZnS ceramics after conventional sintering at 1000°C for 6 h under Ar flow [16]. This interesting result was obtained thanks to an advanced forming techniques of slip casting in combination with cold isostatic pressing of nanosized powder. The mean grain size of the resulting ceramics was around 4 µm, highlighting an important grain growth during sintering. Earlier, Fujita and Nitta obtained 94 % dense ZnS ceramics after conventional sintering at 1000 °C with barium chloride as additive [17]. $BaCl_2$ was found to react with ZnS to form Ba_2ZnS_3. Densification then occurs by liquid phase sintering. Our own tests confirmed this result and a huge grain growth was also observed. Dense ZnS ceramics with good optical properties are thus mainly obtained by hot-pressing (HP) or chemical vapor deposition (CVD) followed by hot isostatic pressing (HIP) post treatment [18-20]. However, these methods are time-consuming and therefore expensive, and also lead to microstructure with grain size much bigger than 1 µm (and up to 20 µm by CVD), even when nanopowders were used as starting material [10,21-23]. Spark plasma sintering (SPS) is a recent consolidation technique that offers the possibility to fully densify a wide range of various materials while retaining the submicronic structures at low sintering temperatures [24]. In the SPS process, the powdered materials are loaded in a graphite die-punches system, uniaxially pressed, and directly heated by pulsed direct currents passing through the graphite assembly. These specific features allow high heating and cooling rates. Several authors successfully applied this method to sinter ZnS ceramics between 750 °C and 900 °C [25-27]. The relative density is close to the theoretical value and the mean grain sizes ranges from 500 nm to more than 10 µm. The objective of this work is to optimize the SPS processing of ZnS nanopowders in order to obtain nanostructured dense ceramics (*i.e.* grain size < 100 nm) with enhanced hardness.

Pure nanocrystalline ZnS powder fabricated using an industrially scalable proprietary process (coprecipitation method) was used. A very weak signal of S-O bonds was detected by FTIR. Powder was characterized by SEM (SU-70 Hitachi SEM-FEG), TEM (FEI G2 operating at 120 kV) and XRD (Bruker D8-Advance diffractometer with Cu-Kα radiation source, λ_1 = 1.54056 Å and λ_2 = 1.54439 Å, equipped with a LynxEye detector). Rietveld refinements were performed using the FullProf program [28]. Specific surface area of the raw powder was measured by the BET method in N_2 with a Belsorp-Max apparatus. ZnS powder were sintered under vacuum (around 10 Pa) using a Dr. Sinter 515S Syntex setup belonging to the "Plateforme de Frittage Ile de France" (Thiais, France) in a 10- or 15-mm diameter graphite die under a pressure of 125 MPa. Pressure was applied gradually during the first half of the heating ramp and then held up to the beginning of the cooling step. According to the work of Chen *et al.* who claimed that to reduce the content of hexagonal wurtzite in the ZnS ceramics the heating rate in the SPS process should be reduced, the heating ramp was fixed to 25 °C.min^{-1} [26]. Each SPS experiment was performed twice in order to check the reproducibility. Bulk density of the sintered pieces was determined by the Archimedes method in water. The relative density of each specimen was calculated as the quotient of bulk density to theoretical density (d_{th} = 4.09 g.cm^{-3}). Standard deviation, estimated from repeated experiments was around 0.75 %. Microstructures of the sintered pellets were observed by SEM upon fresh fractures. The surface of the samples was coated with a 5 nm layer of Pt prior to observation. For each sample, approximately 400 grains were analyzed. Microhardness was measured on polished ceramics using a Vickers microhardness tester (Buehler VH1102). Microhardness *Hv* was determined using the following equation:

$$H_v = k\left(\frac{P}{d^2}\right) \quad (1)$$

where *P* is the applied load (500 g, *i.e.* 4.903 N), *k* the shape factor (0.1891) and *d* the indent diagonal (mm). All the final results represent the average of 20 indentation tests.

The as-received powder is mainly composed of cubic ZnS, with some traces of the hexagonal form (XRD pattern of Fig. 1-a). The cell parameter is 0.5407(2) nm (density: 4.09). Fig. 1 shows that the powder consists of agglomerates in the range of 10 to 15 μm in size (b). Agglomerates are made of nanoparticles of 50 to 60 nm (c). TEM observation (d) highlights crystalline domains of around 20 nm, which is very consistent with the domain size calculated with the Scherrer formula on the (220) peak (20 nm). The specific surface area of the powder is 38 $m^2.g^{-1}$.

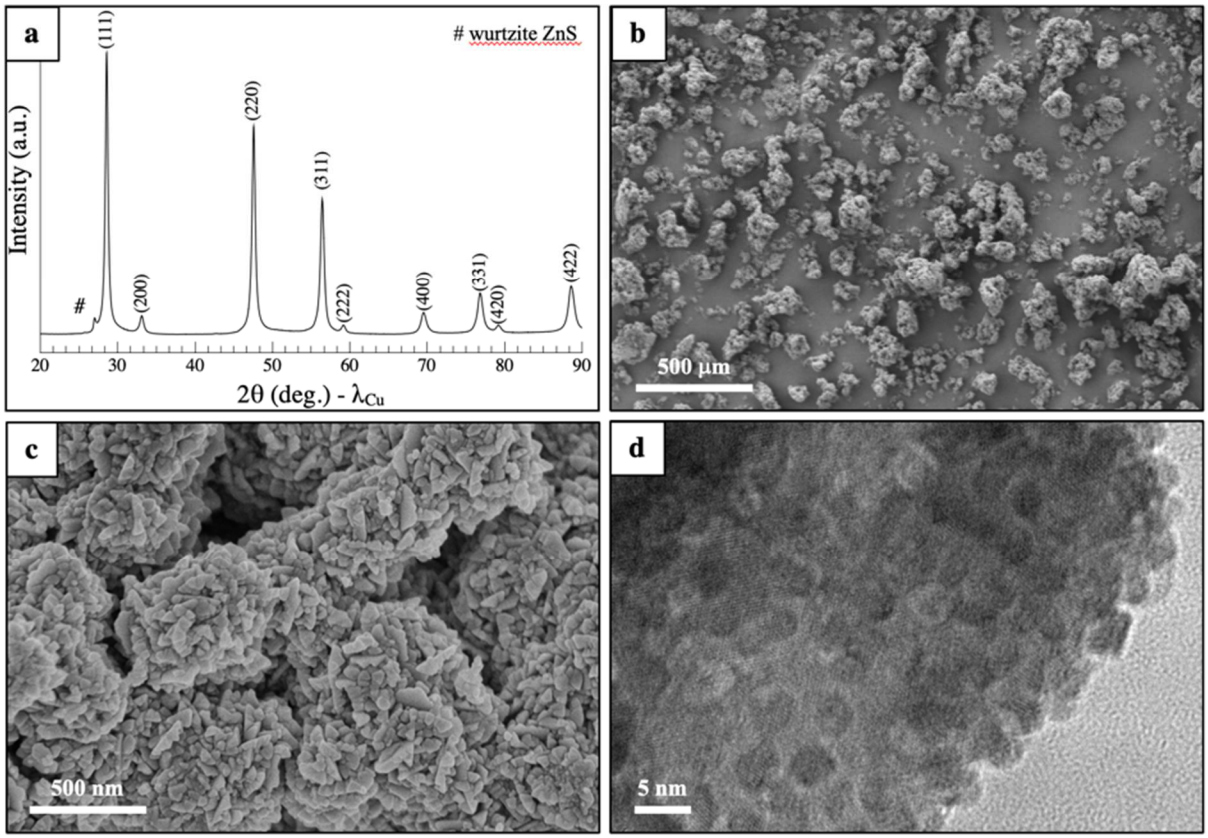

Fig. 1. XRD pattern (a) and morphology (b and c: SEM; d: TEM) of the as-received ZnS nanopowder

Fig. 2-a shows the relative density and the mean grain size of ZnS ceramics sintered by SPS under a pressure of 125 MPa with a heating rate of 25 °C.min^{-1} and a dwell time of 1 min. Maximum densification (98.2 % of the theoretical density) is obtained at a temperature

as low as 550 °C. For higher temperatures, a slight decrease of the relative density is observed (96.7 % at 900 °C). Grain growth is quite negligible during the densification. After sintering at 550 °C for 1 min, mean grain size is around 75 nm (Fig. 3). Grain size distribution is homogeneous and follows a log-normal law. As far as we know, this is the first time that almost fully dense ZnS ceramics with such a small grain size are reported. When sintering temperature increases above 600 °C, a huge grain growth is observed. This grain growth is responsible of the de-densification observed at high temperature, *via* a mechanism of pore coalescence during the final stage of sintering [29,30]. Indeed, the gas pressure in the resulting big pores is significantly lower than in the starting nanopores, so the total pore volume increases. It is worth noting that the microstructure of ZnS ceramics sintered at temperature higher than 700 °C consists in round-shaped big grains (Fig. 3 - 900 °C). In these samples, fracture mainly occurs via a transgranular crack growth mechanism, whereas only intergranular fracture can be observed for ceramics sintered at lower temperature (*i.e.* ceramics with very smaller grain size).

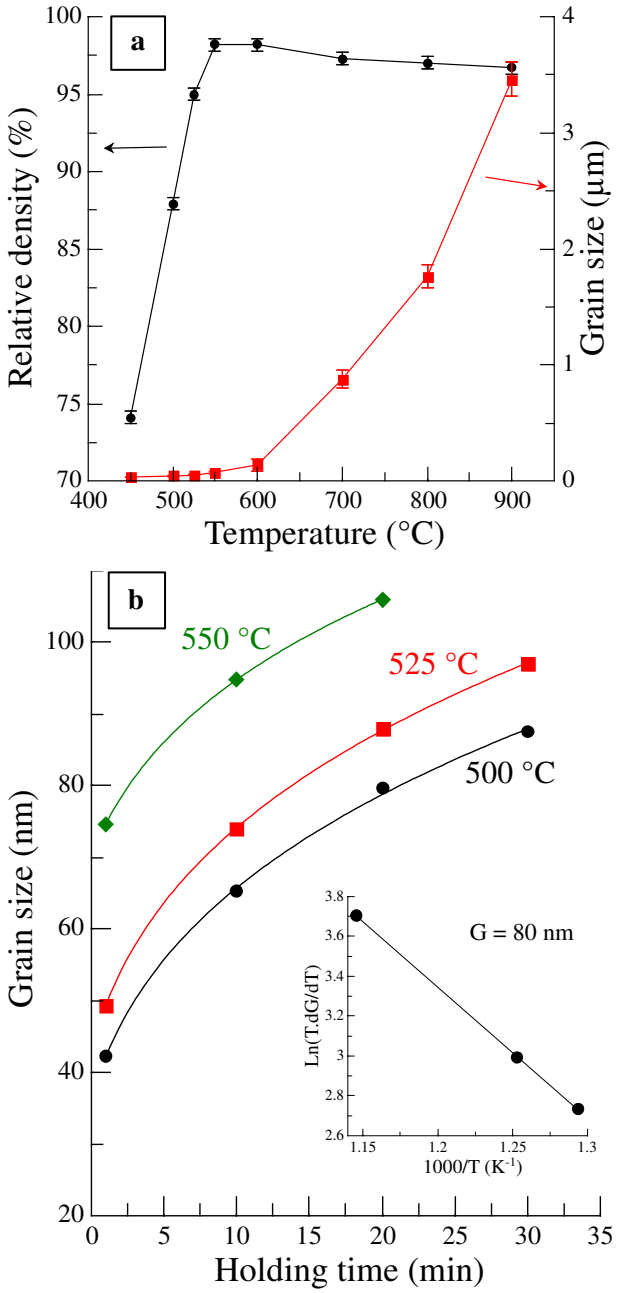

Fig. 2. (a) Relative density, mean grain size (dwell time of 1 min) and (b) isothermal grain growth (inset: related Arrhenius plot at a grain size G = 80 nm) of ZnS ceramics sintered by SPS under 125 MPa with a heating rate of 25 °C.min^{-1}

Grain growth kinetic was investigated by isothermal experiments conducted in the range 500 °C – 550 °C. Experimental results can be modeled assuming a normal grain growth

in a nearly fully dense material, through the following kinetic equation, proposed by Brook and transposed to spark plasma sintering of nanocrystalline ceramics by Chaim *et al.* [31-33]:

$$G^n - G_0^n = k(T)t \quad (2)$$

where

$$k(T) = \frac{k_0}{T} \mathrm{e}^{-E_G/RT} \quad (3)$$

In Eqs. (2) and (3), G is the grain size ($G = G_0$ at time $t = 0$), n is a constant representative of the grain growth mechanism, k is the kinetic constant, inversely proportional to the temperature T, k_0 is the pre-exponential term, R is the universal gas constant and E_G is the activation energy of the process controlling grain growth.

The activation energy is thus deduced from the slope of the plot $\ln(T(\mathrm{d}G/\mathrm{d}t) = f(1/T)$ at a given grain size G:

$$\ln\left(T\frac{\mathrm{d}G}{\mathrm{d}t}\right)_{\mathrm{G}} = -\frac{E_G}{R}\frac{1}{T} + \mathrm{A} \quad (4)$$

where A is a constant. n exponents deduced from Eq. (2) are 3.4, 3.7 and 4.8 (± 0.2) for 500 °C, 525 °C and 550 °C, respectively. Values at 500 °C and 525 °C are very consistent with that measured by Yin *et al.* (3.7) [16], who suggests that grain growth occurs by a combination of volume and surface diffusion [35]. Note that, as in the case of the Yin *et al.* paper, the samples sintered at 525 °C and 550 °C are not fully dense (85 and 95 %, respectively). In these conditions, the use of Eq. (2), based on the hypothesis of a near fully dense material, is not perfectly appropriate. The sample sintered at 550 °C exhibits a relative density higher than 98 %. The corresponding n value is more reliable and shows that surface diffusion is the predominant mechanism [35]. The fast grain growth observed at temperature higher than 550 °C is concomitant with the disappearance of porosity, highlighting than below this temperature, grain growth kinetic is controlled by pore drag effect.

For a given grain size G = 80 nm, the activation energy is 54.4 ± 0.3 kJ.mol^{-1}. This value is low compared to other systems (*e.g.* 224 to 461, 382, 150 and 1078 kJ.mol^{-1} for ZnO

[35], Ce_2S_3 [36], Y_2O_3 [32] and TaB_2 [37], respectively) and is consistent with the huge increase of the grain growth kinetic with the temperature observed in our samples.

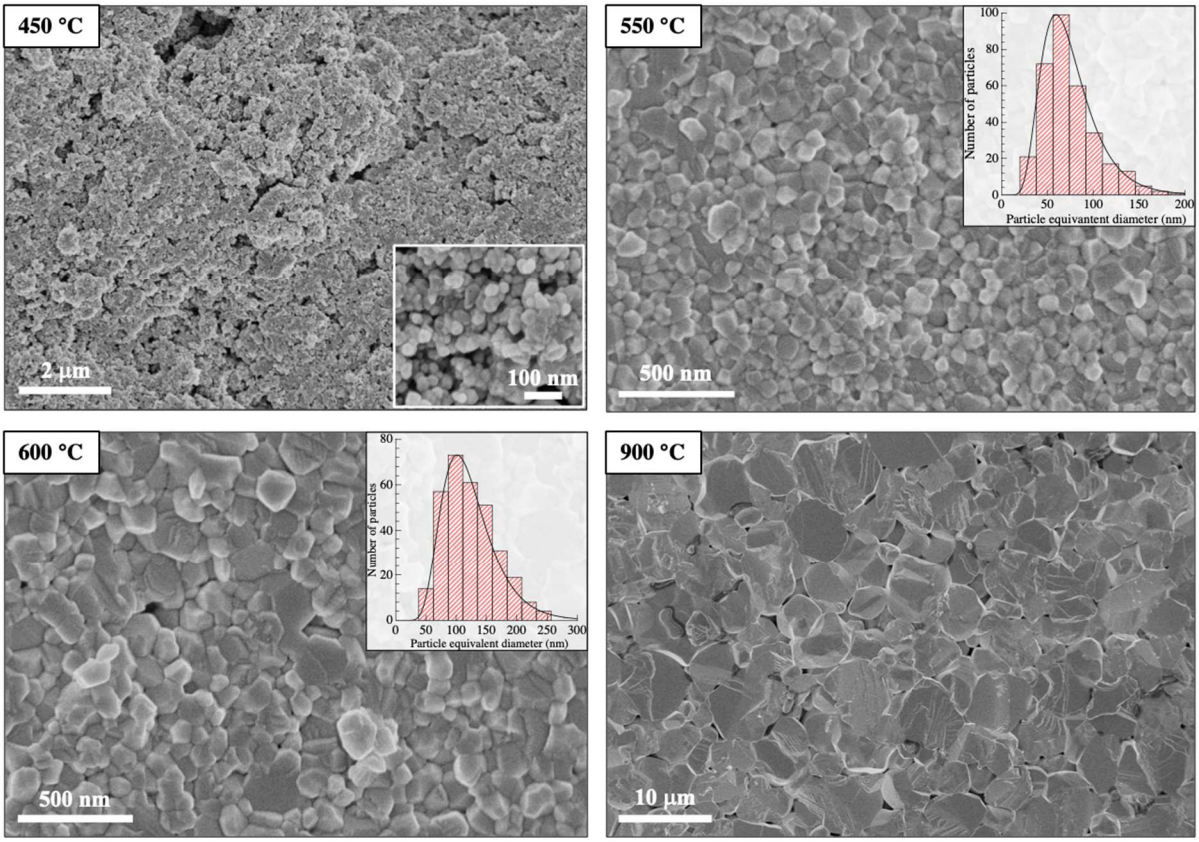

Fig. 3. Fracture and grain size distribution of ZnS ceramics sintered by SPS at different temperature under 125 MPa for 1 min with a heating rate of 25 °C.min^{-1}

Vickers hardness values of the sintered ZnS ceramics are plotted as a function of the sintering temperature and the mean grain size on the graphs of Fig. 4. Our own values are compared to that found in the literature on CDV ZnS ceramics [10,39]. Maximum of hardness (4.2 ± 0.1 GPa) is obtained for the sample with the maximum relative density and the smaller grain size (*i.e.* sintered at 525 and 550 °C). As far as we known, our samples show the higher hardness reported to date for ZnS ceramics.

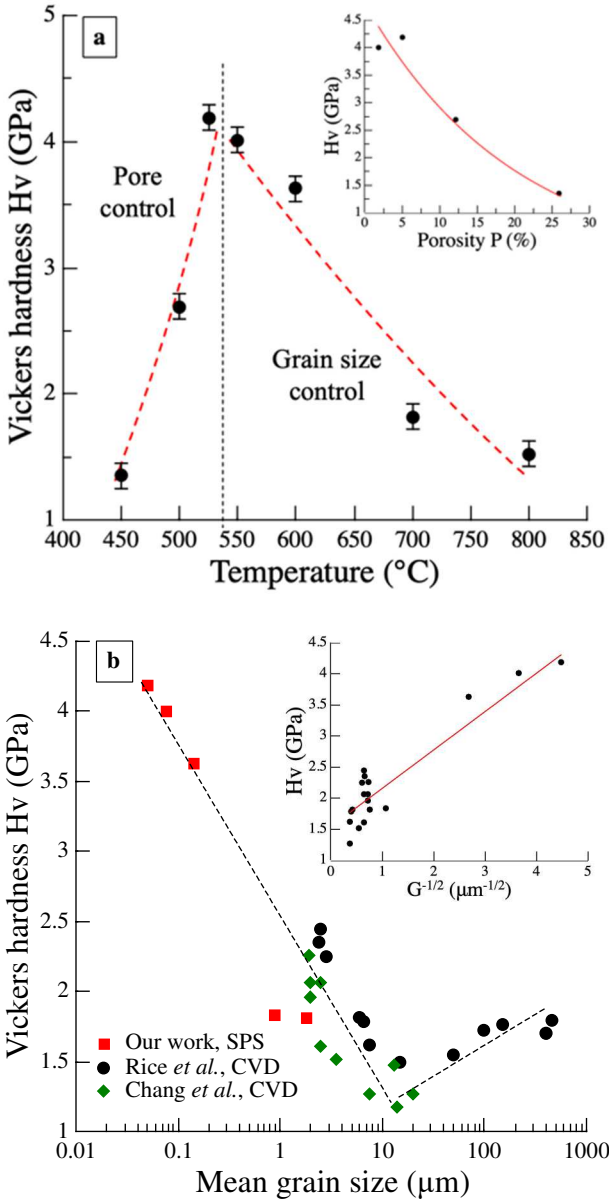

Fig. 4. Vickers hardness value *vs* sintering temperature and porosity (a) and *vs* mean grain size (b) of ZnS ceramics

For sample sintered below 525 °C, hardness is controlled by the porosity P (Fig. 4-a, inset), following an exponential trend [40,41]:

$$H_v = H_0 \exp(-bP) \quad (6)$$

with H_0 = 4.8 GPa (hardness for a fully dense sample) and b = 0.05.

For sample sintered at a temperature higher than 550 °C, an important decrease of microhardness is observed, due to the huge grain growth previously described. The

relationship between grain size and hardness was already observed on ZnS ceramics made by CVD [39]. Our samples with grain size around 1 μm exhibit lower hardness than that observed in the literature because they are not fully dense on the contrary of the sample made by CVD. Combined with the results reported in the literature, grain size effect on hardness can be modeled with the Hall-Petch law [42]:

$$H_v = H_\infty + \frac{K}{\sqrt{G}} \quad (7)$$

with H_v, K and G the Vickers hardness, the strengthening constant and the mean grain size, respectively (H_∞ = 1.5 GPa (hardness for a sample with a supposed infinite grain size) and K = 0.6 GPa.m^{½}).

In conclusion, we show that almost fully dense ZnS ceramics with grain size lower than 100 nm can be obtained by using SPS process on nanopowders only if the sintering temperature remains low enough to avoid the fast grain growth mechanism to take place. The control of the nanometric grain size of the final microstructure is of prime importance to improve the hardness of ceramics, and hardness of 4.2 GPa can be obtained, which is 70 % higher than the current state of the art. Even if this value is still much lower than that of other IR ceramics (13.6, 20 and 18 GPa for $MgAl_2O_4$ [43], Al_2O_3 [44] and AlON [45], respectively), this strong improvement in hardness is significant and confirms that ZnS transparent ceramic is a credible candidate for IR windows. Improvement of the whole process (*i.e.* shaping and sintering) should allow the fabrication of ultrafine grains transparent ZnS ceramics with improved mechanical properties.

CRediT author statement

Damien Bregiroux: Conceptualization, Methodology, Resources, Investigation, Data curation, Writing- Original draft preparation. Julie Cedelle: Visualization, Investigation, Writing- Reviewing and Editing.

Declaration of Competing Interest

The authors declare that they have no known competing financial interests or personal relationships that could have appeared to influence the work reported in this paper.

Acknowledgements

The authors are grateful to David Montero for SEM observations on the SEM-FEG instrumentation of the IMPC FR2482 (Institut des Matériaux de Paris Centre) and funded by Sorbonne Université, CNRS and by the C'Nano projects of the Région Ile-de-France.

Data availability

The raw/processed data required to reproduce these findings are available upon request.

References

[1] I.T. Steinberger, Prog. Cryst. Growth Charact. Mater. 7 (1983) 7-5.

[2] J. Baars, G. Brandt, J. Phys. Chem. Solids 34 (1973) 905-909.

[3] P.C. Lin, C.C. Hua, T.C. Lee, J. Solid State Chem. 194 (2012) 282-285.

[4] X. Fang, T. Zhai, U. K. Gautam, L. Li, L. Wu, Y. Bando, D. Golberg, Prog. Mater. Sci. 56 (2011) 175-287.

[5] A. Jaffres, D. Bregiroux, D. Reekie, R. Shears, Mater. Lett. 209 (2017) 539-542.

[6] C. B. Willingham, J. Pappis, Polycrystalline zine sulphide and zinc selenide articles having improved optical quality, U. S. Patent: 4944900 (1990).

[7] E.V. Yashina, Inorg. Mater. 39 (2003) 663-668.

[8] R.H. Page, K.I. Schaffers, L.D. DeLoach, G.D. Wilke, F.D. Patel, J.B. Tassano, S.A. Payne, W.F. Krupke, K.-T. Chen, A. Burger, IEEE J. Quant. Elect. 33 (1997) 609-619.

[9] Q. Zhong, H. Kou, L. Yang, Y. Tao, C. Luo, Z. Xu, Mater. Lett. 158 (2015) 222-224.

[10] C.S. Chang, J.L. He, Z.P. Lin, Wear 255 (2003) 115-120.

[11] S.F. Wang, J. Zhang, D.W. Luo, F. Gu, D.Y. Tang, Z.L. Dong, G.E.B. Tan, W.X. Que, T.S. Zhang, S. Li, L.B. Kong, Prog. Solid State Chem. 41 (2013) 20-54.

[12] T. Mroz, L. M. Goldman, A. D. Gledhill, D. Li, N. P. Padture, Int. J. Appl. Ceram. Technol. 9 (2012) 83-90.

[13] D. Bregiroux, J. Cedelle, I. Ranc, C. Barreteau, G. Mata Osoro, G. Wallez, J. Phys. Chem. Solids 111 (2017) 304-310.

[14] P. Ramavath, V. Mahender, U.S. Hareesh, R. Johnsona, S. Kumari, N. Eswara Prasad, Mater. Sci. Eng. A 528 (2011) 5030-5035.

[15] Y.-D. Kim, K. Sonezaki, H. Maeda, A. Kato, J. Mater. Sci. 32 (1997) 5101-5106.

[16] J. Yin, Y. Li, Y. Wu, Ceram. Int. 42 (2016) 11504-11508.

[17] Y. Fujita, T. Nitta, J. Am. Ceram. Soc. 65 (1982) C18-C19.

[18] P. Biswas, R. Senthil Kumar, P. Ramavath, V. Mahendar, G.V.N. Rao, U.S. Hareesh, R. Johnson, J. Alloys Compd 496 (2010) 273-277.

[19] C. Li, T. Xie, H. Kou, Y. Pan, J. Li, J. Eur. Ceram. Soc. 37 (2017) 2253-2257.

[20] A. Abdi, F. Davar, Ceram. Inter. 46 (2020) 21107-21119.

[21] C. Chlique, O. Merdrignac-Conanec, N. Hakmeh, X. Zhang, J.-L. Adam, J. Am. Ceram. Soc. 96 (2013) 3070-3074.

[22] Y. Li, Y. Wu, J. Am. Ceram. Soc. 98 (2015) 2972-2975.

[23] K.T. Lee, B.H. Choi, J.U. Woo, J.S. Kang, J.H. Paik, B.U. Chu, S. Nahm, J. Eur. Ceram. Soc. 38 (2018) 4237-4244.

[24] N. Poirot, D. Bregiroux, P. Boy, C. Autret-Lambert, P. Belleville, L. Bianchi, Ceram. Inter. 41 (2015) 3879-3887.

[25] C. Chlique, G. Delaizir, O. Merdrignac-Conanec, C. Roucau, M. Dollé, P. Rozier, V. Bouquet, X.H. Zhang, Opt. Mater. 33 (2011) 706-712.

[26] Y. Chen, L. Zhang, J. Zhang, P. Liu, T. Zhou, H. Zhang, D. Gong, D. Tang, D. Shen, Opt. Mater. 50 (2015) 36-39.

[27] J.W. Hong, W.K. Jung, D.H. Choi, Ceram. Inter. 46 (2020) 16285-16290.

[28] J. Rodriguez-Carvajal, FULLPROF.2k: Rietveld, Profile Matching and Integrated Intensity Refinement of X-ray and Neutron Data, V 1.9c, Laboratoire Léon Brillouin, CEA, Saclay, France, 2001.

[29] U.C. Oh, Y.S. Chung, D.Y. Kim, J. Am. Ceram. Soc. 71 (1988) 854-857.

[30] Suk-Joong Kang, Sintering: Densification, Grain Growth and Microstructure, Butterworth-Heinemann Ltd (2014).

[31] R.J. Brook, Controlled Grain Growth, in: Ceramic fabrication processes, Treatise on Materials Science and Technology, vol. 9 F.F.Y. Wang (Ed.), Academic Press, New York, 1976, p331.

[32] R. Chaim, Mater. Sci. Eng. A 443 (2007) 25-32.

[33] R. Chaim, A. Shlayer, C. Estournes, J. Eur. Ceram. Soc. 29 (2009) 91-98.

[34] M. N. Rahaman, Ceramic Processing and Sintering, second ed., Marcel Dekker, New York 2003.

[35] S. Deng, T. Yuan, R. Li, F. Zeng, G. Liu, X. Zhou, Powder Technol. 310 (2017) 264-271.

[36] B. Yuksel, T. Osman Ozkan, Mater. Sci.-Poland 33 (2015) 220-229.

[37] S. Hirai, K. Shimakage, Y. Saitou, T. Nishimura, Y. Uemura, M. Mitomo, L. Brewer, J. Am. Ceram. Soc. 81 (1998) 145-151.

[38] D. Demirskyi, O. Vasylkiv, Ceram. Int. 42 (2016) 16396-16400.

[39] R.W. Rice, C.C. Wu, F. Borchelt, J. Am. Ceram. Soc. 77(10) (1994) 2539-2553.

[40] Dean, E. A. and Lopez, J. A., J. Am. Ceram. Soc., 1983, 66(5), 366-370.

[41] L. Perrière, D. Bregiroux, B. Naitali, F. Audubert, E. Champion, D.S. Smith, D. Bernache-Assollant, J. Eur. Ceram. Soc. 27 (2007) 3207-3213.

[42] N.A. Gaida, N. Nishiyama, O. Beermann, U. Schürmann, A. Masuno, C. Giehl, K. Niwa, M. Hasegawa, S. Bhat, R. Farla, L. Kienle, Int. J. Ceram. Eng. Sci. 2 (2020) 76–82.

[43] Y. Liu, J. Zhu, Ceram. Int. 46 (2020) 4154-4158.

[44] K.-Y. Lee, C.-C. Chen, H.-I Hsiang, F.-S. Yen, C.-Y. Huang, Int. J. Appl. Ceram. Technol. 16 (2019) 1493-1500.

[45] M. Ding, T. Wang, B. Maerz, S. Robertson, Z. Sun, L. Fan, Y. Shi, H. Wu, Ceram. Int. 45 (2019) 21127-21135.